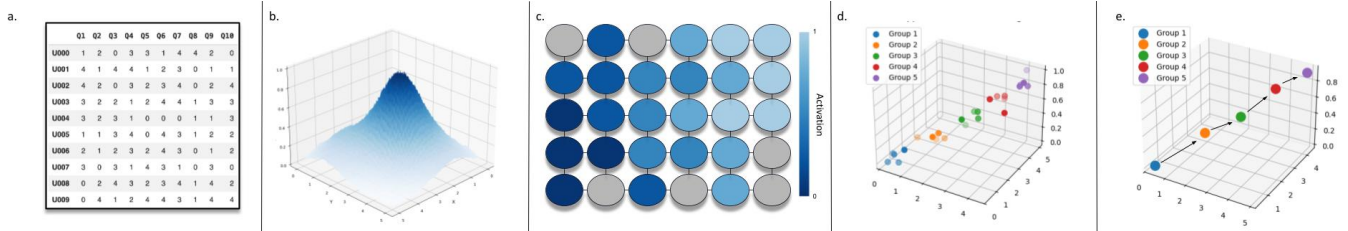


# SOMtime the World Ain't Fair: Violating Fairness Using Self-Organizing Maps

Joseph Bingham\*  
jbingham@campus.technion.ac.il  
Technion-Israel Institute of  
Technology  
Haifa, Israel

Netanel Arussy  
narussy@campus.technion.ac.il  
Technion-Israel Institute of  
Technology  
Haifa, Israel

Dvir Aran  
dviraran@technion.ac.il  
Technion-Israel Institute of  
Technology  
Haifa, Israel



**Figure 1: The SOMtime pipeline.** (a) High-dimensional tabular data with sensitive attributes withheld. (b) A high-capacity Self-Organizing Map learns a topology-preserving discretization. (c) Activation patterns across the SOM lattice. (d) Observations mapped to a 3D embedding (BMU coordinates + activation energy), colored by withheld sensitive attribute (age group). For attributes with simple progression, the SOM embedding arranges observations along a monotonic axis aligned with the withheld sensitive attribute, revealing information leakage invisible to standard methods. (e) Trajectory of ordered centroid progressions of protected values recovered from downstream analysis.

## Abstract

Unsupervised representations are widely assumed to be neutral with respect to sensitive attributes when those attributes are withheld from training. We show that this assumption is false. Using SOMtime, a topology-preserving representation method based on high-capacity Self-Organizing Maps, we demonstrate that sensitive attributes such as age and income emerge as dominant latent axes in purely unsupervised embeddings, even when explicitly excluded from the input. On two large-scale real-world datasets (the World Values Survey across five countries and the Census-Income dataset), SOMtime recovers monotonic orderings aligned with withheld sensitive attributes, achieving Spearman correlations of up to 0.85, whereas PCA and UMAP typically remain below 0.23 (with a single exception reaching 0.31), and against t-SNE and autoencoders which achieve at most 0.34. Furthermore, unsupervised segmentation of SOMtime embeddings produces demographically skewed clusters, demonstrating downstream fairness risks without any supervised task. These findings establish that *fairness through unawareness* fails at the representation level for ordinal sensitive attributes and that fairness auditing must extend to unsupervised

\*Corresponding authors

Permission to make digital or hard copies of all or part of this work for personal or classroom use is granted without fee provided that copies are not made or distributed for profit or commercial advantage and that copies bear this notice and the full citation on the first page. Copyrights for components of this work owned by others than the author(s) must be honored. Abstracting with credit is permitted. To copy otherwise, or republish, to post on servers or to redistribute to lists, requires prior specific permission and/or a fee. Request permissions from [permissions@acm.org](mailto:permissions@acm.org).

KDD '25, Toronto, ON, Canada

© 2025 Copyright held by the owner/author(s). Publication rights licensed to ACM.  
ACM ISBN 978-1-4503-XXXX-X/2025/08  
<https://doi.org/XXXXXXX.XXXXXXX>

components of machine learning pipelines. We have made the code available at <https://github.com/JosephBingham/SOMtime/>

## CCS Concepts

• **Computing methodologies** → **Machine learning**; *Neural networks*; • **Applied computing** → *Law, social and behavioral sciences*.

## Keywords

fairness, unsupervised learning, self-organizing maps, sensitive attribute leakage, dimensionality reduction

## ACM Reference Format:

Joseph Bingham, Netanel Arussy, and Dvir Aran. 2025. SOMtime the World Ain't Fair: Violating Fairness Using Self-Organizing Maps. In *Proceedings of the 31st ACM SIGKDD Conference on Knowledge Discovery and Data Mining (KDD '25)*. ACM, New York, NY, USA, 10 pages. <https://doi.org/XXXXXXX.XXXXXXX>

## 1 Introduction

Modern machine learning pipelines increasingly rely on unsupervised representations as foundational building blocks. Clustering, dimensionality reduction, and learned embeddings are used for customer segmentation, data exploration, visualization, and as pre-processing steps for downstream prediction [23]. These representations are often assumed to be neutral, particularly when sensitive attributes such as age, gender, race, or income are deliberately withheld from the input features.

This assumption, known as *fairness through unawareness* [7], has been widely critiqued in the supervised learning literature. It is well established that models can reconstruct sensitive attributes from correlated proxy features, leading to discriminatory outcomes even

when the protected variable is absent from the training data [14, 26]. However, the fairness community has focused predominantly on supervised predictors, i.e. classifiers and regressors with explicit outcome labels [23]. Comparatively little attention has been paid to whether *unsupervised* representations themselves encode sensitive information, and if so, how severely.

The presence of this gap is not trivial for end-users who are assuming their usage of unsupervised embedding prevents any fairness issues. When an unsupervised embedding systematically organizes data along a sensitive axis, any downstream use of that embedding (whether for clustering, recommendation, visualization, or feature extraction) inherits a fairness risk *before any supervised task is even defined*. Recent work in recommender systems has confirmed that collaborative filtering embeddings can capture user demographics even when demographic features are not provided [8]. Fair clustering research has shown that standard algorithms produce demographically imbalanced partitions [6, 9]. And studies of fair dimensionality reduction have demonstrated that methods like t-SNE can produce visualizations dominated by sensitive-attribute structure [25].

In this work, we make four contributions:

**Empirical demonstration of sensitive-attribute recoverability.** We show that unsupervised representations encode sensitive attributes (age, income) with high fidelity, even when those attributes are excluded from training.

**A topology-based auditing method.** We propose SOMtime, based on high-capacity Self-Organizing Maps [16], as an unsupervised audit tool that reveals *global* sensitive structure, including monotonic orderings and gradients, that is attenuated or invisible in standard embeddings (PCA [20], UMAP [22], t-SNE [29]).

**Comparative evidence against common baselines.** We show that SOM-based representations leak substantially more sensitive information than PCA, UMAP, t-SNE, and autoencoders despite all methods being fully unsupervised.

**Implications for fairness beyond supervised learning.** We argue that fairness interventions must operate at the representation level and include unsupervised components, motivating new auditing and mitigation strategies.

We study this phenomenon empirically on two large, real-world datasets: the World Values Survey (WVS) [11], a globally representative survey of political and moral values used in recent top-tier ML publications [2, 17, 33], and the Census-Income (KDD) dataset [1]. In both cases, we withhold sensitive attributes entirely from the representation learning process and measure the degree to which they emerge as dominant latent structure.

Our results show that SOMtime achieves Spearman correlations up to 0.85 between its learned embedding axes and withheld sensitive attributes, whereas PCA and UMAP typically remain below 0.23 (with a single exception reaching 0.31). Moreover, unsupervised segmentation of SOMtime embeddings produces clusters with substantial demographic skew, demonstrating that fairness risks arise even in the absence of any supervised objective.

## 2 Background and Related Work

### 2.1 Fairness Beyond Supervised Learning

The principle of *fairness through unawareness*, the idea that removing sensitive attributes from model inputs suffices to prevent discrimination, has been extensively studied and shown to be insufficient [7, 18]. Proxy features correlated with protected attributes can enable models to reconstruct the withheld information and reproduce discriminatory patterns [23]. While this critique is well established for supervised learning, its implications for unsupervised representations have received less attention.

Recent surveys document a growing body of work on fairness in machine learning [23, 26], yet the vast majority of proposed fairness criteria (demographic parity, equalized odds, calibration [14]) are defined with respect to outcome labels and are therefore specific to supervised tasks. The question of whether unsupervised representations are “fair” remains underexplored.

### 2.2 Fairness in Unsupervised Learning

*Fair Clustering.* The seminal work of Chierichetti et al. [6] introduced *fairlets*, small balanced subsets used as preprocessing to ensure demographic balance in cluster assignments. Subsequent work extended fair clustering to  $k$ -center and  $k$ -means objectives with group-balance constraints [3, 15], and Ghadiri et al. [9] proposed socially fair clustering that minimizes the maximum group-specific cost. Chhabra et al. [5] provide a comprehensive survey of fairness in clustering.

*Fair Representation Learning.* A complementary line of work focuses on learning latent representations that are predictive of useful features but uninformative of protected attributes. Zemel et al. [32] proposed learning fair representations via an optimization objective that balances accuracy and demographic parity. Adversarial approaches [21, 31] train an encoder jointly with an adversary that attempts to predict the sensitive attribute from the latent code; the encoder is penalized when the adversary succeeds. The Variational Fair Autoencoder [19] uses Maximum Mean Discrepancy to match latent distributions across groups. Concept erasure methods [27] post-process representations by projecting out directions correlated with sensitive attributes.

Beyond fairness-specific variants, standard autoencoders are widely used as general-purpose nonlinear dimensionality reduction tools [12] and are commonly employed as representation learning baselines in fairness auditing studies. Their ability to learn continuous, distributed latent codes with controllable bottleneck dimensionality makes them a natural point of comparison for any method claiming to expose latent structure.

*Fair Dimensionality Reduction.* Samadi et al. [28] studied the “price of fair PCA,” showing that equal reconstruction error across groups can be achieved by increasing the target dimensionality by one. Peltonen et al. [25] introduced fairness-aware objectives for nonlinear embeddings, showing that standard t-SNE can produce visualizations dominated by sensitive-attribute structure. Conditional t-SNE [13] generates embeddings that factor out specified structure.

*Auditing for Sensitive-Attribute Leakage.* A common auditing approach is the *probing classifier*: train a simple predictor on learned representations to assess whether a sensitive attribute can be recovered [23]. High prediction accuracy signals information leakage. This technique is standard for evaluating fair representation learning but has primarily been applied to supervised embeddings. Complementary approaches based on mutual information estimation [24] provide a more general measure of statistical dependence but are computationally more demanding and less interpretable for continuous ordinal attributes.

### 2.3 Topology-Preserving Representations and the Fairness Gap

Self-Organizing Maps (SOMs), introduced by Kohonen [16], learn topology-preserving discretizations of high-dimensional data onto a lattice of prototype vectors. While SOMs were widely used for clustering and visualization, they have seen little treatment in recent fairness literature [10, 26]. Modern fairness research has focused on deep learning and differentiable embeddings, leaving classical topology-preserving methods largely unexamined.

Critically, prior work on fairness in unsupervised learning focuses primarily on *local separability* (whether groups can be locally distinguished) or *classification leakage* (whether a probing classifier can predict group membership). We identify a distinct and previously unaddressed risk: **global geometric ordering**. When an unsupervised representation arranges observations along a monotonic axis aligned with a sensitive attribute, this constitutes a form of structured leakage that is qualitatively different from local separability. Standard low-dimensional embeddings (PCA, UMAP) attenuate this signal; high-capacity SOMs amplify it.

We show that topology-preserving maps with sufficient capacity expose a global fairness risk that projection- and reconstruction-based methods systematically obscure.

## 3 Method: SOMtime as a Tool

We position SOMtime not as a solution to fairness, but as a *lens* that makes sensitive structure in unsupervised representations explicit. The method reveals whether and how strongly a representation encodes withheld sensitive attributes.

### 3.1 Problem Setup

We consider a dataset-agnostic unsupervised setting. Each observation is a fixed-length feature vector  $\mathbf{x}_i \in \mathbb{R}^d$ , optionally associated with a sensitive attribute  $s_i$  that is **withheld** from all representation learning. The goal is to assess whether  $s$  is encoded in the learned representation, and if so, how strongly.

Crucially, all representation learning steps are fully unsupervised with respect to  $s$ . Sensitive attributes are used **only for post-hoc auditing** via correlation analysis.

### 3.2 Self-Organizing Map Representation

We map the input data into a two-dimensional discrete latent space using a Self-Organizing Map (SOM). Let  $X \in \mathbb{R}^{N \times d}$  denote the input matrix. The SOM consists of a square lattice of  $K \times K$  units, where each unit  $j$  is associated with a prototype vector  $\mathbf{w}_j \in \mathbb{R}^d$ .

For each input observation  $\mathbf{x}_i$ , the best-matching unit (BMU) is defined as

$$j^* = \arg \min_j \|\mathbf{x}_i - \mathbf{w}_j\|.$$

Prototype vectors are updated according to

$$\mathbf{w}_j(t+1) = \mathbf{w}_j(t) + \alpha(t) h(j, j^*, t) (\mathbf{x}_i - \mathbf{w}_j(t)),$$

where  $\alpha(t)$  is a learning rate and  $h(\cdot)$  is a Gaussian neighborhood function defined over the lattice topology. This competitive-learning rule induces a topology-preserving discretization of the data manifold: nearby neurons in the lattice specialize to similar regions of the input space.

In contrast to conventional SOM usage for two-dimensional visualization, we employ a map with a large number of neurons ( $K = 5 \cdot N^{0.54}$ ). This scaling follows a slight modification the heuristic proposed by Vesanto and Alhoniemi [30], which balances representational capacity against computational cost. The resulting lattice allows the SOM to approximate the data distribution at finer granularity than is typical in visualization applications.

### 3.3 Continuous 3D Embedding

To enable continuous analysis of latent structure, we transform the discrete SOM grid into a three-dimensional coordinate system. Each observation inherits the  $(x, y)$  coordinates of its BMU on the lattice, and a third coordinate  $z_i = \|\mathbf{x}_i - \mathbf{w}_{j^*}\|$ , the per-observation quantization error (distance to the BMU prototype). This results in an embedding  $\mathbf{z}_i \in \mathbb{R}^3$  that preserves local neighborhood relations while enabling global geometric analysis.

This 3D embedding allows detection of smooth sensitive-attribute gradients across the representation, including monotonic orderings, neighborhood composition analysis, and structured demographic patterns.

### 3.4 Latent Sensitive-Axis Recovery

To assess whether the learned representation encodes a global ordering aligned with a sensitive attribute, we analyze the induced geometry of SOM unit centroids. We construct an adjacency graph  $G = (V, E)$  over the  $K \times K$  lattice, where each vertex is an index for row and column, and values of the graph are boolean identifiers of edge existence from row to column vertices. Before this algorithm, cluster centers from the SOM distance map are calculated in XY-space. Those XY centroids are then mapped to their point on the SOM distance map to get the centroid activations. Algorithm 1 takes in these centroids to compute ordering and directionality of the trajectories. Edges are computed using a combination of initial ordering from the activation of nodes, followed by a euclidean distance in 3-dimensional space to find the closest node for trajectory. As seen in Algorithm 1 the values in XYZ-space, where Z is the activation, are scaled to emphasize differences in activation. The resulting adjacency graph gives the trajectories of our sensitive attributes.

We formalize the notion of sensitive structure we aim to detect. A representation exhibits *global geometric ordering* with respect to a sensitive attribute  $s$  if there exists a path through the embedding along which  $s$  varies monotonically. This is distinct from *local separability*, which measures whether observations with similar  $s$  values are nearby in the embedding (e.g., via  $k$ -NN purity). A

representation may exhibit high local separability without global ordering—for instance, if age groups form distinct clusters that are randomly arranged in space—or global ordering without local separability. We quantify ordering strength via the Spearman correlation  $\rho$  between  $s$  and position along the recovered path; higher  $|\rho|$  indicates stronger global alignment.

---

**Algorithm 1** Trajectory Adjacency Matrix Construction
 

---

**Require:**  $C \in \mathbb{R}^{n \times 3}$        $\triangleright$  Centroids in form  $(x, y, z = \text{activation})$   
**Require:**  $K \in \mathbb{R}$        $\triangleright$  Dimension of SOM  
**Ensure:**  $A \in \{0, 1\}^{n \times n}$        $\triangleright$  Adjacency matrix of trajectories

```

1:  $A \leftarrow \mathbf{0}_{n \times n}$        $\triangleright$  Initialize adjacency matrix
2: // Trajectory computation
3: for  $i = 1$  to  $n$  do
4:   if  $\sum_k A_{k,i} > 0$  or  $\sum_k A_{i,k} > 0$  then
5:     continue       $\triangleright$  Skip if already connected
6:   end if
7:    $d_{\min} \leftarrow \infty$ 
8:    $j^* \leftarrow -1$ 
9:   for  $j = 1$  to  $n$  do
10:    if  $i = j$  then
11:      continue
12:    end if
13:    // Scale coordinates
14:     $\tilde{c}_i \leftarrow \left( \frac{C_{i,1}}{\sum_{k=1}^n C_{k,1}}, \frac{C_{i,2}}{\sum_{k=1}^n C_{k,2}}, K \cdot C_{i,3} \right)$ 
15:     $\tilde{c}_j \leftarrow \left( \frac{C_{j,1}}{\sum_{k=1}^n C_{k,1}}, \frac{C_{j,2}}{\sum_{k=1}^n C_{k,2}}, K \cdot C_{j,3} \right)$ 
16:     $d \leftarrow \|\tilde{c}_i - \tilde{c}_j\|_2$        $\triangleright$  Euclidean distance
17:    if  $d < d_{\min}$  and  $C_{i,3} < C_{j,3}$  then
18:       $j^* \leftarrow j$ 
19:       $d_{\min} \leftarrow d$ 
20:    end if
21:  end for
22:  if  $j^* \neq -1$  then
23:     $A_{i,j^*} \leftarrow 1$        $\triangleright$  Create trajectory from  $i$  to  $j^*$ 
24:  end if
25: end for
26: return  $A$ 

```

---

If this ordering correlates strongly with a withheld sensitive attribute, the representation has encoded that attribute as emergent structure, constituting a fairness risk.

### 3.5 Auditing via Correlation Analysis

We assess alignment between the learned representation and the withheld sensitive attribute  $s$  by computing Pearson and Spearman correlation coefficients between  $s$  and each of the three embedding dimensions independently. We report the maximum absolute correlation across dimensions. This maximum captures the worst-case leakage: if *any* axis of the embedding is aligned with the sensitive attribute, the representation poses a fairness risk regardless of the other axes. Both Pearson (linear) and Spearman (monotonic) coefficients are reported to capture different forms of dependence.

This evaluation is *purely diagnostic*:  $s$  is never used during training, embedding construction, or ordering extraction.

### 3.6 Why High-Capacity SOMs Reveal Hidden Sensitive Structure

We now explain why SOM-based representations expose sensitive information that projection-based methods systematically attenuate. The key insight is that signals correlated with sensitive attributes in the tabular datasets we consider can be expected to exhibit one or more of the following properties, based on the nature of survey and census data where responses are individually weak proxies for demographic variables:

- Low marginal variance relative to dominant nuisance factors,
- Nonlinear interactions between dimensions,
- Locality on the data manifold rather than global separability,
- Distribution across multiple coordinates without alignment to a single axis.

These characteristics pose fundamental challenges for methods that rely on global variance maximization (PCA), low-dimensional embedding (UMAP), or pairwise similarities of distributions (t-SNE), but are naturally accommodated by the SOM architecture.

**Limitations of PCA** PCA seeks an orthogonal linear transformation that maximizes retained variance. While optimal under linear Gaussian assumptions, this introduces an inductive bias that prioritizes high-variance directions. Signals correlated with sensitive attributes that have low variance relative to other factors are discarded or suppressed. Moreover, PCA is inherently linear and therefore incapable of representing nonlinear or locally varying structure. In the settings considered here, these limitations lead to the systematic attenuation of sensitive-attribute signals.

**Limitations of UMAP** UMAP constructs a low-dimensional embedding by preserving local neighborhood relationships. Although effective for visualization, it imposes a strict low-dimensional bottleneck that necessarily collapses multiple regions of the original space into shared coordinates. Distances in the embedding are not metric-preserving, and the stochastic nature of the optimization can lead to instability across runs. Consequently, UMAP prioritizes visual separability rather than faithful retention of all latent structure, including sensitive-attribute gradients.

**Limitations of t-SNE** t-SNE constructs embeddings by matching probability distributions over pairwise similarities in high and low dimensions, using a Student-t distribution in the embedding space to alleviate crowding. Unlike topology-preserving methods with fixed embedding structures, t-SNE provides neither global distance preservation nor deterministic mappings. Each optimization produces a different layout depending on initialization and hyper-parameters (particularly perplexity). The method offers no explicit coordinate system or grid structure, making it difficult to interpret absolute positions or compare embeddings across datasets. Furthermore, t-SNE lacks an out-of-sample extension, requiring complete re-optimization when new data arrive, and its emphasis on exaggerating local cluster separation can obscure continuous gradients associated with sensitive attributes that would be preserved in ordered topological representations.

**Limitations of Autoencoders** Autoencoders learn nonlinear mappings through an encoder-decoder architecture that minimizes reconstruction error. While they can in principle capture complex manifold structure, their training objective is fundamentally

reconstruction-oriented: the encoder is optimized to retain whatever information the decoder needs to reproduce the input, without any preference for how that information is organized in the latent space. Consequently, signals correlated with sensitive attributes may be encoded diffusely across latent dimensions rather than concentrated along interpretable axes. This distributional encoding preserves the information in a form that is accessible to downstream supervised extraction (e.g., probing classifiers) but does not produce the geometric organization — monotonic orderings, smooth gradients across a fixed lattice — that makes sensitive structure visible and actionable without supervision. The SOM’s competitive learning rule, by contrast, imposes a fixed topological structure that forces the representation to organize observations spatially, converting distributed correlations into coherent geometric patterns.

**Absence of Variance-Based Filtering in SOMs.** Unlike PCA, SOM training does not rank or discard dimensions based on global variance. All input dimensions contribute equally to similarity computations and prototype updates. Signals correlated with sensitive attributes, even those with low marginal variance, are preserved if they are locally consistent.

**Local Nonlinear Approximation.** The SOM represents the data manifold as a collection of locally linear regions rather than a single global projection. This enables it to capture nonlinear dependencies between features and sensitive attributes that linear methods like PCA cannot express.

**Distributed Signal Amplification.** When the lattice resolution is sufficiently high, weak signals that are individually subtle can produce coherent activation patterns across neighboring neurons. These patterns manifest as structured gradients on the map, effectively amplifying sensitive-attribute signals that projection-based methods treat as noise.

**Avoidance of Projection Collapse.** The SOM does not compress all structure into a fixed low-dimensional coordinate system. Information is retained in the identity and organization of activated neurons, mitigating the many-to-one collapse inherent in low-dimensional embeddings like UMAP.

## 4 Experimental Protocol

### 4.1 Implementation Details

All experiments are implemented in Python using standard scientific computing libraries. Hyperparameters for the SOM are fixed across all experiments and are not tuned using sensitive attribute labels:  $\sigma = 0.7$ , learning rate = 0.75, with lattice dimension  $K = 5 \cdot N^{0.54}$ , where  $N$  is the number of inputs. A selection criteria implemented here for determining questions to be used was that the data does not contain missing values. This design ensures that reported correlations reflect emergent structure rather than supervised optimization. Since all of SOM, t-SNE, and UMAP involve stochastic initialization, all reported results are averaged over five independent runs; standard deviations were below 0.03 for all Spearman correlations, indicating stable results.

### 4.2 Datasets

**World Values Survey (WVS)** The WVS [11] is a globally representative dataset capturing political, cultural, and moral values, recently used in top-tier ML venues [2, 17, 33]. We use data from

**Table 1: Correlation of questions from World Value Survey and Census (KDD) datasets and the sensitive attribute of age. For each dataset, the correlation of the most highly correlated question and the average correlation across all used questions are given. Additionally, the number of responses for each data subset is included.**

Dataset	Domain	Max	Mean	Responses
WVS [33]	Canada	-0.35	-0.09	4,018
	Romania	-0.15	0.03	3,200
	Germany	-0.34	-0.07	1,528
	China	-0.25	-0.05	3,036
	USA	-0.26	-0.07	2,609
Census (KDD) [1]	Age	0.27	-0.05	
	Income	0.12	-0.04	27024
	Capital Gains	0.10	0.07	

five countries: Canada ( $N=4,018$ ), Romania ( $N=3,200$ ), Germany ( $N=1,528$ ), China ( $N=3,036$ ), and USA ( $N=2,609$ ), with **age** as the withheld sensitive attribute. Furthermore, only a subset of questions, a subset of those on ethics and morals for both the surveyed individual as well as those they would pass onto a child, are used. This filters the number of questions down to 22 in total. In table 1, we see the mean correlation of the different features used for the experimentation, justifying our choice for their inclusion.

**Census-Income (KDD)** The Census-Income dataset [1] (also known as the KDD Census-Income dataset) is a standard benchmark from the UCI repository containing 299,285 records with 40 demographic and economic features extracted from the 1994 and 1995 Current Population Surveys. We treat **age**, **income**, and **capital gains** as withheld sensitive attributes. We first removed all columns that did not have easy encoding to numerical/decimal values. We then found that many columns had stronger correlations with age and income, which would make any resulting experiments trivial in terms of recovering them as hidden or sensitive features. Thus, we removed those columns as well. Of the 40 questions, we were left with 25 questions (i.e. columns). Unlike the World Value Survey, missing values did not come encoded with error values with specific meaning so we were not certain of the behavior of the data if we were to simply replace them with -1s as we did with the WVS data. Thus, we removed any input that did not have a missing value. This left us with 27,024 observations to work with, which as we can see from the p-values reported in Table 2, was more than sufficient for statistically significant and meaningful results.

Although removing columns or features that are correlated with the sensitive features would require knowledge beforehand, we chose to include this portion of our preprocessing to give all of the algorithms the hardest possible learning problem to showcase the difference in ability between our method, SOMtime, and all of the other methods that we use as baselines. We only ever use knowledge of the sensitive feature in this context, and after this processing, it is not used at all during training or clustering or any other section of the algorithm until validation.

**Table 2: Sensitive attribute leakage: maximum correlation between any single embedding axis and the withheld sensitive attribute. Pearson and Spearman values may come from different axes; signed values are reported to indicate direction. The  $p$ -values correspond to the Spearman correlation (two-sided test). Higher absolute values indicate greater leakage.  $\epsilon$  is the machine precision of floating points. Best values from ablations used. Standard deviations for 5 runs was below 0.03.**

Dataset	Domain	Method														
		PCA			UMAP			t-SNE			AE			SOMtime		
		Pear.	Spear.	$p$	Pear.	Spear.	$p$	Pear.	Spear.	$p$	Pear.	Spear.	$p$	Pear.	Spear.	$p$
WVS [33]	Canada	-0.25	0.22	$1.94 \cdot 10^{-48}$	-0.31	0.31	$2.86 \cdot 10^{-90}$	-0.22	-0.21	$4.77 \cdot 10^{-42}$	0.33	0.34	$1.91 \cdot 10^{-108}$	0.75	0.85	$\leq \epsilon$
	Romania	0.06	0.04	0.05	-0.06	-0.05	$1.35 \cdot 10^{-3}$	0.06	0.05	$2.42 \cdot 10^{-3}$	0.16	0.15	$1.33 \cdot 10^{-18}$	0.66	0.59	$2.25 \cdot 10^{-8}$
	Germany	-0.16	-0.18	$8.24 \cdot 10^{-13}$	0.17	0.19	$2.02 \cdot 10^{-14}$	0.19	-0.35	$1.37 \cdot 10^{-15}$	-0.29	-0.29	$2.07 \cdot 10^{-31}$	0.79	0.73	$1.47 \cdot 10^{-12}$
	China	-0.22	-0.22	$8.10 \cdot 10^{-35}$	0.21	0.20	$4.11 \cdot 10^{-31}$	0.24	-0.23	$1.84 \cdot 10^{-39}$	0.19	0.25	$4.98 \cdot 10^{-46}$	0.80	0.58	$1.58 \cdot 10^{-8}$
	USA	-0.20	-0.23	$1.87 \cdot 10^{-49}$	-0.33	-0.34	$7.30 \cdot 10^{-72}$	0.25	-0.24	$6.71 \cdot 10^{-36}$	0.27	0.29	$8.10 \cdot 10^{-50}$	0.80	0.52	$1.51 \cdot 10^{-8}$
Census (KDD) [1]	Age	0.17	0.11	$5.26 \cdot 10^{-9}$	0.08	0.09	$7.72 \cdot 10^{-6}$	0.08	-0.10	$3.75 \cdot 10^{-7}$	-0.20	-0.22	$7.44 \cdot 10^{-31}$	0.50	0.83	$\leq \epsilon$
	Income	-0.31	0.21	$1.34 \cdot 10^{-27}$	0.07	0.07	$1.14 \cdot 10^{-4}$	-0.08	-0.08	$4.15 \cdot 10^{-5}$	0.22	0.25	$6.96 \cdot 10^{-39}$	0.48	0.69	$\leq \epsilon$
	Capital Gains	-0.23	-0.11	$5.26 \cdot 10^{-9}$	0.01	0.002	0.89	-0.02	0.04	$4.92 \cdot 10^{-3}$	0.35	0.40	$5.32 \cdot 10^{-4}$	0.34	0.43	0.01

### 4.3 Baselines

We compare SOMtime against four widely used unsupervised dimensionality reduction techniques: **PCA**: A 50-dimensional linear embedding computed via standard principal component analysis. **UMAP**: A 50-dimensional nonlinear embedding computed using Uniform Manifold Approximation and Projection with default parameters. **t-SNE**: A 50-dimensional nonlinear embedding computed using t-distributed Stochastic Neighbor Embedding, optimized to preserve local neighborhood structure. **Autoencoder AE**: Nonlinear embeddings computed via encoder-decoder networks trained to minimize reconstruction error. To control for representational capacity, we evaluate autoencoders at three scales: small ( $\approx 7K$  parameters), medium ( $\approx 95K$  parameters), and large ( $\approx 1.4M$  parameters), each with bottleneck dimensionalities of 3, 10, and 22. The large configuration is capacity-matched to the SOM, enabling direct comparison without the confound that the SOM’s advantage stems solely from higher capacity.

All three methods are run independently as separate baselines. Although we performed elbow tests to look at the optimal number of components needed for each of these baselines, we chose to go with 50 dimensions each in order to avoid any worries that the only reason our method, SOMtime, does better is because it has a higher capacity to learn than the other methods due to its dimensionality, rather than something inherent to its formulation. We find that 50 dimensions is more than enough to have the same computational capacity and learning resources as our dimension of SOM, based on the literature [4]. We ran the same experiments with the standard numbers of dimensions (2-3), the optimal number (using the elbow method), and the full 50 only to find their results were within 2% of one another, meaning for the sake of this work, all of these values are interchangeable. We also performed a full ablations on hyperparameters of these methods (e.g. perplexity, learning rate, etc) and selected the best values for each. For autoencoders, we additionally vary the bottleneck dimensionality (3, 10, 22) and network capacity (small, medium, large) to disentangle the effects of compression, nonlinearity, and total representational capacity from the topology-preserving properties specific to the SOM.

Further classification was not implemented on the dimensionality reduced data. A probing classifier requires labeled sensitive attributes to train and evaluate, making it a supervised auditing tool. In contrast, SOMtime reveals sensitive structure as an *emergent geometric property of the representation*, without access to sensitive labels at any stage. While sensitive attributes may be extractable using such classifiers, SOMtime shows that information is already organized in the representation in a way that affects any downstream use — clustering, visualization, or feature extraction — regardless of whether the user intends to exploit it. The threat model is different: we demonstrate ambient leakage, not ability to extract.

Further, even though we look *only* at one dimension of the resulting embedding of SOMtime (i.e. only the activation, or Z-axis), we look over *every* dimension of the resulting embedding for the other methods. We choose to look at each dimension independently rather than utilizing some linear combination or probe of each embedding because to know which would be the most successful in a real world application requires knowledge of the sensitive value, whereas we show we can recover them without any access to the sensitive values with SOMtime.

### 4.4 Experiments

**Experiment 1: Sensitive Attribute Recoverability.** For each method (PCA, UMAP, t-SNE, AE, SOMtime), we compute the embedding with the sensitive attribute withheld entirely. We then measure the maximum Pearson and Spearman correlation between any embedding axis and the sensitive attribute. Higher correlation indicates greater information leakage.

**Experiment 2: Global Ordering Emergence.** We extract the dominant 1D latent axis from each representation (Strongest principal component for t-SNE/PCA/UMAP/AE and *only* looking at the Z-axis for SOMtime) and compute its Spearman correlation with the sensitive attribute. This experiment specifically tests whether each method recovers a *monotonic global ordering*, the form of leakage that distinguishes SOMtime from baselines.

**Experiment 3: Recovering Sensitive Topology from 3D Embedding.** To demonstrate the risk to fairness embedded in the data,

we construct full trajectory-based ordering of the sensitive attribute of age in the 3D embedding, beyond the known age groupings. Not only do we find which group each individual belongs to, but also the relative positions of the groups within the SOM embedding. This experiment shows the risk of bias from underlying sensitive attributes recoverable from non-sensitive data. This ordering serves as a proxy for alternative downstream tasks, as it creates a pseudo-classifier, much like how an SVM or other method would be trained on the embedding data.

## 5 Results

### 5.1 Sensitive Attribute Leakage

Table 2 presents the core results. Across all datasets and sensitive attributes, SOMtime achieves higher correlations with the withheld sensitive attribute than either PCA or UMAP. On the WVS dataset, SOMtime attains Spearman correlations of 0.43-0.85 with age across five countries, while PCA, UMAP, t-SNE, and AE achieve at most 0.34. On the Census dataset, SOMtime achieves Spearman correlations of 0.83 (age), compared to maxima of 0.22 for the baselines.

A natural question is whether SOMtime's higher sensitive-attribute correlation simply reflects higher overall representational fidelity. We note that the SOM's effective representational capacity ( $K^2$  prototype vectors) far exceeds that of a 3D linear or nonlinear embedding, making it unsurprising that more structure is preserved overall. However, the magnitude of the gap is notable: sensitive-attribute correlations increase by a factor of 3–8 $\times$  over baselines. Whether this reflects preferential amplification of sensitive structure or proportional preservation of all structure is an empirical question that requires measuring reconstruction quality for non-sensitive attributes as well, which we leave to future work.

These results demonstrate that topology-preserving representations with sufficient capacity encode sensitive attributes far more strongly than projection-based methods, even when those attributes are entirely withheld from training. For Capital Gains, the gap between SOMtime and AE narrows substantially, suggesting that both approach a floor imposed by the underlying data.

A natural concern is whether SOMtime's advantage reflects the SOM's higher parameter count rather than its topological inductive bias. To address this, we evaluated autoencoders at three capacity scales, see Appendix B. The large autoencoder (1.4M parameters) with a 22-dimensional bottleneck achieves near-perfect reconstruction ( $MSE = 0.001$ ) yet attains a maximum Spearman correlation of only 0.34 with age, comparable to UMAP 0.31 and far below SOMtime 0.85. Critically, increasing autoencoder capacity does not improve sensitive-attribute recovery: for the 3-dimensional bottleneck, the small autoencoder (7K) achieves 0.29, while the large autoencoder (1.4M) achieves only 0.19. This inverse relationship between capacity and per-axis sensitive correlation indicates that the phenomenon we observe is specific to the SOM's competitive learning dynamics and fixed lattice, which concentrate distributed sensitive signals into a geometric structure rather than its size.

We did not apply trajectory-based ordering to baseline embeddings, as seen for SOMtime in Figure 2 and Table 3, because analysis revealed that clustering these representations did not produce centroids with systematic sensitive-attribute structure. This absence of

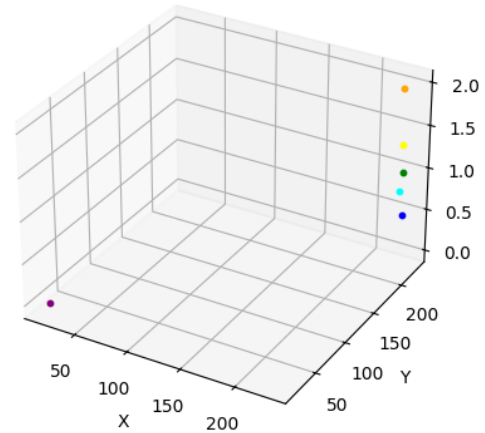


**Figure 2: Example of sensitive attribute emergence SOMtime. Age groups form a monotonic ordering along the learned surface. Colors: purple (youngest)  $\rightarrow$  blue  $\rightarrow$  green  $\rightarrow$  yellow  $\rightarrow$  orange (oldest). Cyan: non-respondents. This global ordering constitutes information leakage invisible to PCA, UMAP, t-SNE, and AE.**

recoverable centroid ordering is itself evidence that global geometric structure is not present in PCA, UMAP, t-SNE, or autoencoder embeddings—the trajectory algorithm has nothing to find.

### 5.2 Global Ordering Emergence

Figure 2 visualizes the SOM embedding for the WVS dataset, with observations colored by age group (withheld during training). The age groups form a clear monotonic ordering along the SOM's latent surface. Note that the cyan markers represent non-respondents. These are randomly distributed near the center of the embedding, consistent with the absence of age-related signal.

To quantify this effect, we extracted the dominant 1D axis from each representation (best principal component of the embedding for PCA, UMAP, t-SNE, and AE); the graph diameter path for SOMtime) and computed its Spearman correlation with age. On the WVS Canada subset, SOMtime achieves  $\rho = 0.85$ , compared to at most  $\rho = 0.34$  with AE. Results are qualitatively similar across countries and the Census dataset. PCA and UMAP produce embeddings in which age groups overlap substantially and no monotonic axis is recoverable, whereas the SOM's topology-preserving competitive learning, combined with high lattice resolution, amplifies the distributed signal of age across many correlated survey responses into a coherent geometric structure.

The SOM models for the World Value Survey dataset were trained individually on a country by country basis. The recovery of age, income, and capital gains from the Census (KDD) dataset was done with a singular SOM. We calculated the correlations here as age to income being -0.11, income to capital gains being 0.07, and age to capital gains being 0.15, showing that despite their low correlation values there are multiple underlying sensitive attributes to be recovered in non-sensitive data. Capital Gains shows that this algorithm does not recover all sensitive attributes.

**Table 3: Accuracy of Recovered Topology Ordering per Domains. WVS: we omit centroids denoting non-respondents**

Dataset	Domain	Recovery Accuracy
WVS [33]	Canada	1.00
	Romania	1.00
	Germany	1.00
	China	0.60
	USA	0.80
Census (KDD) [1]	Age	0.82
	Income	0.76
	Capital Gains	0.22

These results establish the ability of SOMs to recover sensitive attributes from non-sensitive data with high correlation across multiple domains. While this is not always a perfect recovery, multiple countries were recovered and others saw high recovery still. This resulting high accuracy shows the existence of the sensitive attributes in these datasets and the ability of it to extend to other datasets as these were composed of real-world data. Thus, the risk of bias is demonstrated to be present even in non-sensitive data.

### 5.3 Recovering Sensitive Topology from 3D Embedding

Table 3 shows our accuracy in recovering sensitive attributes groups from non-sensitive data. Accuracy here refers to whether if  $A \rightarrow B$  is present in the ground truth, as would be the case for age group 25 – 35 is followed by 35 – 45 in the data, then this connection should be detected by our Algorithm 1 and reported. If a false one is found, such as a connection from 45 – 55  $\rightarrow$  25 – 30, this is incorrect, and if a correct connection is missing, this is incorrect.

These results show that the SOMs perform well with results mostly being 100% recovery of age for multiple countries. Across these 5 countries from the WVS as well as in the Census (KDD) dataset we recover age with very high accuracy, while in the Census (KDD) dataset Age and Income is also recovered with a high accuracy, 0.82 and 0.76 respectively. This is far higher than if it were randomly guessing edges, which we would be for 5 groups (4 edges), the probability of all 4 correct by chance is  $1/5! = 1/120 \approx 0.008$ .

These results show the risk to those working on downstream tasks. The ability of SOMs to recover, cluster and create topologies of sensitive attributes from non-sensitive data with high fidelity demonstrates the threat it poses. While this isn't always a perfect recovery, multiple countries were recovered perfectly and others saw high recovery still. Thus, the risk of using seemingly uncorrelated, as would be indicated by use of PCA, UMAP, or t-SNE, is clearly demonstrated to be present even in non-sensitive data.

## 6 Discussion

Our results demonstrate that purely unsupervised representations can encode sensitive attributes with high fidelity, and that topology-preserving methods with sufficient capacity are particularly effective at exposing this phenomenon. We frame SOMtime as an *auditing tool* that reveals a problem, not as a solution to it.

We view probing classifiers and SOMtime as complementary rather than competing auditing approaches. Probing classifiers assess worst-case extractability; SOMtime assesses whether sensitive

attributes are a dominant organizing principle of the representation. The latter is more concerning for fairness, since it affects all downstream tasks of the embedding, not only those who actively attempt recovery. The underlying trajectories of sensitive attributes cause the risk to fairness.

## 7 Limitations and Ethical Considerations

**We do not propose a fairness mitigation in this work.** Instead, we identify three concrete directions for future research:

**Representation Auditing as Standard Practice.** Our findings suggest that any unsupervised representation deployed in a decision-making pipeline should be routinely audited for sensitive-attribute leakage. This could involve (a) probing classifier tests, as is standard in the fair representation learning literature [21, 31], and (b) global ordering checks of the kind enabled by SOMtime.

**Regularization for Topology-Preserving Maps.** The SOM training procedure could be augmented with fairness-aware regularization. Possible approaches include penalizing monotonic correlation between axes and sensitive attributes during training, or enforcing demographic entropy on neuron neighborhoods, requiring that each neuron's receptive field contains a balanced mix of demographic, analogous to fairlet constraints [6], which would shift this to a semi-supervised setting.

**Topology-Aware Fairness Constraints.** Beyond regularization, structural constraints on the SOM lattice could be introduced: balancing neuron occupancy across demographic groups, or penalizing smooth sensitive-attribute gradients across the lattice surface. These would extend the principles of fair dimensionality reduction [25, 28] to the discrete, topology-preserving setting of SOMs.

### 7.1 Limitations

Our study focuses on ordinal sensitive attributes (age, income) where monotonic correlation is a natural measure of leakage. For categorical attributes (e.g. race, gender), different auditing metrics would be needed. Additionally, the datasets used (WVS, Census) are tabular; extending these findings to image, text, or graph embeddings is an important direction for future work.

## 8 Conclusion

Unsupervised learning is not neutral. We have shown that purely unsupervised representations can encode withheld sensitive attributes as emergent geometric structure, and that topology-preserving methods like Self-Organizing Maps are particularly effective at revealing this phenomenon. On two large-scale real-world datasets, SOMtime recovered monotonic orderings aligned with age and income that were invisible to PCA, UMAP, t-SNE, and AE, and unsupervised segmentation of these embeddings produced demographically skewed clusters.

These findings carry a clear implication: fairness auditing must extend beyond supervised predictors to the unsupervised representations that increasingly serve as the foundation of modern ML pipelines. We recommend that practitioners adopt representation-level leakage audits, including both correlation-based checks and global ordering analysis, as a standard step before deploying unsupervised embeddings in decision-making contexts. SOMtime provides a practical tool for this purpose, making representation-level fairness risks visible and measurable.

## Acknowledgments

This work was funded by The Technion - Israel Institute of Technology.

## References

- [1] 2000. Census-Income (KDD). UCI Machine Learning Repository. DOI: <https://doi.org/10.24432/C5N30T>.
- [2] Farid Adilazuarda, Chen Cecilia Liu, Iryna Gurevych, and Alham Fikri Aji. 2025. From Surveys to Narratives: Rethinking Cultural Value Adaptation in LLMs. In *Proceedings of the 2025 Conference on Empirical Methods in Natural Language Processing*, Christos Christodoulopoulos, Tanmoy Chakraborty, Carolyn Rose, and Violet Peng (Eds.). Association for Computational Linguistics, Suzhou, China, 18063–18090. doi:10.18653/v1/2025.emnlp-main.912
- [3] Sara Ahmadian, Alessandro Epasto, Ravi Kumar, and Mohammad Mahdian. 2019. Clustering without Over-Representation. In *Proceedings of the 25th ACM SIGKDD International Conference on Knowledge Discovery & Data Mining* (Anchorage, AK, USA) (KDD '19). Association for Computing Machinery, New York, NY, USA, 267–275. doi:10.1145/3292500.3330987
- [4] Hyun-Jung Bae, Jong-Seong Park, Ji-Hyeok Choi, and Hyuk-Yoon Kwon. 2025. Learning model combined with data clustering and dimensionality reduction for short-term electricity load forecasting. *Sci. Rep.* 15, 1 (Jan. 2025), 3575.
- [5] Anshuman Chhabra, Karina Masalkovaitė, and Prasant Mohapatra. 2021. An Overview of Fairness in Clustering. *IEEE Access* 9 (2021), 130698–130720. doi:10.1109/ACCESS.2021.3114099
- [6] Flavio Chierichetti, Ravi Kumar, Silvio Lattanzi, and Sergei Vassilvitskii. 2017. Fair clustering through fairlets. In *Proceedings of the 31st International Conference on Neural Information Processing Systems* (Long Beach, California, USA) (NIPS'17). Curran Associates Inc., Red Hook, NY, USA, 5036–5044.
- [7] Cynthia Dwork, Moritz Hardt, Toniann Pitassi, Omer Reingold, and Richard Zemel. 2012. Fairness through awareness. In *Proceedings of the 3rd Innovations in Theoretical Computer Science Conference* (Cambridge, Massachusetts) (ITCS '12). Association for Computing Machinery, New York, NY, USA, 214–226. doi:10.1145/2090236.2090255
- [8] Michael D Ekstrand and Daniel Kluger. 2021. Exploring author gender in book rating and recommendation. *User Model. User-adapt Interact.* 31, 3, 377–420.
- [9] Mehrdad Ghadiri, Samira Samadi, and Santosh Vempala. 2021. Socially Fair k-Means Clustering. In *Proceedings of the 2021 ACM Conference on Fairness, Accountability, and Transparency* (Virtual Event, Canada) (FAccT '21). Association for Computing Machinery, New York, NY, USA, 438–448. doi:10.1145/3442188.3445906
- [10] Axel Guérin, Pierre Chauvet, and Frédéric Saubion. 2024. A Survey on Recent Advances in Self-Organizing Maps. arXiv:2501.08416 [cs.NE] <https://arxiv.org/abs/2501.08416>
- [11] Christian Haerpfer, Ronald Inglehart, Alejandro Moreno, Christian Welzel, Kseniya Kizilova, Jaime Diez-Medrano, Marta Lagos, Pippa Norris, Eduard Ponarin, and Bi Puraenen. 2020. World Values Survey wave 7 (2017–2020) cross-national data-set.
- [12] G E Hinton and R R Salakhutdinov. 2006. Reducing the dimensionality of data with neural networks. *Science* 313, 5786 (July 2006), 504–507.
- [13] Bo Kang, Dario García García, Jeffrey Lijffijt, Raúl Santos-Rodríguez, and Tijl de Bie. 2021. Conditional t-SNE: More informative t-SNE embeddings. In *2021 IEEE 8th International Conference on Data Science and Advanced Analytics (DSAA)*. 1–2. doi:10.1109/DSAA53316.2021.9564212
- [14] Jon M. Kleinberg, Sendhil Mullainathan, and Manish Raghavan. 2016. Inherent Trade-Offs in the Fair Determination of Risk Scores. *CoRR* abs/1609.05807 (2016). arXiv:1609.05807 <http://arxiv.org/abs/1609.05807>
- [15] Matthäus Kleindessner, Samira Samadi, Pranjal Awasthi, and Jamie Morgenstern. 2019. Guarantees for Spectral Clustering with Fairness Constraints. In *International Conference on Machine Learning*. <https://api.semanticscholar.org/CorpusID:59291890>
- [16] T. Kohonen. 1990. The self-organizing map. *Proc. IEEE* 78, 9 (1990), 1464–1480. doi:10.1109/5.58325
- [17] Cheng Li, Mengzhuo Chen, Jindong Wang, Sunayana Sitaram, and Xing Xie. 2024. CultureLLM: Incorporating Cultural Differences into Large Language Models. In *Advances in Neural Information Processing Systems*, A. Globerson, L. Mackey, D. Belgrave, A. Fan, U. Paquet, J. Tomczak, and C. Zhang (Eds.), Vol. 37. Curran Associates, Inc., 84799–84838. doi:10.52202/079017-2693
- [18] Shuhan Liu, Zheyun Qin, Xuan Hou, Yining Wang, Ziwen Wang, and Zhaohui Peng. 2026. Fairness-aware graph representation learning through bias disentanglement. *Information and Software Technology* 193 (2026), 108034. doi:10.1016/j.infsof.2026.108034
- [19] Christos Louizos, Kevin Swersky, Yujia Li, Max Welling, and Richard Zemel. 2017. The Variational Fair Autoencoder. arXiv:1511.00830 [stat.ML] <https://arxiv.org/abs/1511.00830>
- [20] Andrzej Mackiewicz and Waldemar Ratajczak. 1993. Principal components analysis (PCA). *Comput. Geosci.* 19, 3 (March 1993), 303–342.
- [21] David Madras, Elliot Creager, Toniann Pitassi, and Richard S. Zemel. 2018. Learning Adversarially Fair and Transferable Representations. *CoRR* abs/1802.06309 (2018). arXiv:1802.06309 <http://arxiv.org/abs/1802.06309>
- [22] Leland McInnes, John Healy, and James Melville. 2020. UMAP: Uniform Manifold Approximation and Projection for Dimension Reduction. arXiv:1802.03426 [stat.ML] <https://arxiv.org/abs/1802.03426>
- [23] Ninareh Mehrabi, Fred Morstatter, Nripsuta Saxena, Kristina Lerman, and Aram Galstyan. 2021. A Survey on Bias and Fairness in Machine Learning. *ACM Comput. Surv.* 54, 6, Article 115 (July 2021), 35 pages. doi:10.1145/3457607
- [24] Daniel Moyer, Shuyang Gao, Rob Brekelmans, Greg Ver Steeg, and Aram Galstyan. 2018. Invariant representations without adversarial training. In *Proceedings of the 32nd International Conference on Neural Information Processing Systems* (Montreal, Canada) (NIPS'18). Curran Associates Inc., Red Hook, NY, USA, 9102–9111.
- [25] Jaakko Peltonen, Wen Xu, Timo Nummenmaa, and Jyrki Nummenmaa. 2023. Fair Neighbor Embedding. In *Proceedings of the 40th International Conference on Machine Learning* (Proceedings of Machine Learning Research, Vol. 202), Andreas Krause, Emma Brunskill, Kyunghyun Cho, Barbara Engelhardt, Sivan Sabato, and Jonathan Scarlett (Eds.). PMLR, 27564–27584. <https://proceedings.mlr.press/v202/peltonen23a.html>
- [26] Ricardo Trainotti Rabonato and Lilian Berton. 2024. A systematic review of fairness in Machine Learning. *AI and Ethics* 5, 3 (Sep 2024), 1943–1954. doi:10.1007/s43681-024-00577-5
- [27] Shauli Ravfogel, Yanai Elazar, Hila Gonen, Michael Twiton, and Yoav Goldberg. 2020. Null It Out: Guarding Protected Attributes by Iterative Nullspace Projection. In *Proceedings of the 58th Annual Meeting of the Association for Computational Linguistics*, Dan Jurafsky, Joyce Chai, Natalie Schluter, and Joel Tetreault (Eds.). Association for Computational Linguistics, Online, 7237–7256. doi:10.18653/v1/2020.acl-main.647
- [28] Samira Samadi, Uthaiapon Tao Tantipongpipat, Jamie Morgenstern, Mohit Singh, and Santosh S. Vempala. 2018. The Price of Fair PCA: One Extra Dimension. *CoRR* abs/1811.00103 (2018). arXiv:1811.00103 <http://arxiv.org/abs/1811.00103>
- [29] Laurens van der Maaten and Geoffrey Hinton. 2008. Visualizing Data using t-SNE. *Journal of Machine Learning Research* 9, 86 (2008), 2579–2605. <http://jmlr.org/papers/v9/vandermaaten08a.html>
- [30] J. Vesanto and E. Alhoniemi. 2000. Clustering of the self-organizing map. *IEEE Transactions on Neural Networks* 11, 3 (2000), 586–600. doi:10.1109/72.846731
- [31] Yutaka Matsuo Yusuke Iwasawa, Kotaro Nakayama. 2018. Censoring Representations with Multiple-Adversaries over Random Subspaces. <https://openreview.net/forum?id=ByuP8yZrB>
- [32] Rich Zemel, Yu Wu, Kevin Swersky, Toni Pitassi, and Cynthia Dwork. 2013. Learning Fair Representations. In *Proceedings of the 30th International Conference on Machine Learning* (Proceedings of Machine Learning Research, Vol. 28), Sanjoy Dasgupta and David McAllester (Eds.). PMLR, Atlanta, Georgia, USA, 325–333. <https://proceedings.mlr.press/v28/zemel13.html>
- [33] Wenlong Zhao, Debanjan Mondal, Niket Tandon, Danica Dillion, Kurt Gray, and Yuling Gu. 2024. WorldValuesBench: A Large-Scale Benchmark Dataset for Multi-Cultural Value Awareness of Language Models. arXiv:2404.16308 [cs.CL] <https://arxiv.org/abs/2404.16308>

## A GenAI Disclosure

LLMs were used to assist with editing and grammar of text. All ideas, concepts, results, and writing/running of code was done by humans alone.

## B Ablation Study of AE Size

**Table 4: Autoencoder capacity ablation across all datasets (age as withheld sensitive attribute for WVS; age and income for Census). Maximum per-axis  $|\rho|$  Spearman correlation. Reconstruction MSE on standardized features shown in parentheses. Despite near-perfect reconstruction at large scale, autoencoders do not approach SOMtime’s sensitive-attribute recovery. Increasing capacity does not consistently improve leakage.**

Model	Params	Bneck	WVS (Age)					Census (KDD)	
			Canada	Romania	Germany	China	USA	Age	Income
<i>Small autoencoders (~7–9K params)</i>									
AE-small	7K	3d	0.29 (0.446)	0.09 (0.419)	0.28 (0.434)	0.25 (0.372)	0.25 (0.469)	0.20 (0.168)	0.17 (0.168)
AE-small	8K	10d	0.19 (0.152)	0.08 (0.164)	0.24 (0.148)	0.23 (0.116)	0.24 (0.163)	0.17 (0.009)	0.13 (0.009)
AE-small	9K	22d	0.28 (0.031)	0.13 (0.022)	0.22 (0.063)	0.25 (0.023)	0.20 (0.054)	0.20 (0.001)	0.18 (0.001)
<i>Medium autoencoders (~91–97K params)</i>									
AE-medium	94K	3d	0.22 (0.304)	0.10 (0.262)	0.23 (0.297)	0.19 (0.246)	0.29 (0.342)	0.18 (0.073)	0.15 (0.073)
AE-medium	95K	10d	0.21 (0.065)	0.08 (0.047)	0.28 (0.047)	0.23 (0.039)	0.22 (0.075)	0.19 (0.001)	0.08 (0.001)
AE-medium	97K	22d	0.23 (0.004)	0.09 (0.005)	0.28 (0.014)	0.21 (0.006)	0.25 (0.013)	0.21 (0.001)	0.22 (0.001)
<i>Large autoencoders (~1.4M params)</i>									
AE-large	1.4M	3d	0.19 (0.124)	0.05 (0.075)	0.25 (0.108)	0.23 (0.105)	0.23 (0.150)	0.22 (0.014)	0.14 (0.014)
AE-large	1.4M	10d	0.24 (0.002)	0.11 (0.002)	0.26 (0.003)	0.19 (0.002)	0.26 (0.002)	0.20 (0.0002)	0.25 (0.0002)
AE-large	1.4M	22d	0.34 (0.001)	0.15 (0.001)	0.29 (0.002)	0.23 (0.002)	0.27 (0.002)	0.21 (0.0001)	0.17 (0.0001)
<b>SOMtime</b>			<b>0.85</b>	<b>0.59</b>	<b>0.73</b>	<b>0.58</b>	<b>0.52</b>	<b>0.83</b>	<b>0.69</b>
SOM params			4.28M	3.35M	1.51M	3.16M	2.66M	2.05M	2.05M

Values shown as  $|\rho|_{\text{Spearman}}$  (Recon. MSE). All  $p$ -values  $< 0.01$ .